

---

# PVO: Panoptic Visual Odometry

---

Weicai Ye<sup>1\*</sup>   Xinyue Lan<sup>1\*</sup>   Shuo Chen<sup>1</sup>   Yuhang Ming<sup>2</sup>   Xingyuan Yu<sup>1,3</sup>

Hujun Bao<sup>1</sup>

Zhaopeng Cui<sup>1</sup>

Guofeng Zhang<sup>1†</sup>

<sup>1</sup>State Key Lab of CAD&CG, Zhejiang University

<sup>2</sup>Visual Information Laboratory, University of Bristol

<sup>3</sup>Wuhan University

{weicaiye, xinyuelan, chenshuo.eric, baohujun, zhpcui, zhangguofeng}@zju.edu.cn  
yuhang.ming@bristol.ac.uk.   RickyYXY@whu.edu.cn

## Abstract

We present a novel panoptic visual odometry framework, termed PVO, to achieve a more comprehensive modeling of the scene’s motion, geometry, and panoptic segmentation information. PVO models visual odometry (VO) and video panoptic segmentation (VPS) in a unified view, enabling the two tasks to facilitate each other. Specifically, we introduce a panoptic update module into the VO module, which operates on the image panoptic segmentation. This Panoptic-Enhanced VO module can trim the interference of dynamic objects in the camera pose estimation by adjusting the weights of optimized camera poses. On the other hand, the VO-Enhanced VPS module improves the segmentation accuracy by fusing the panoptic segmentation result of the current frame on the fly to the adjacent frames, using geometric information such as camera pose, depth, and optical flow obtained from the VO module. These two modules contribute to each other through a recurrent iterative optimization. Extensive experiments demonstrate that PVO outperforms state-of-the-art methods in both visual odometry and video panoptic segmentation tasks. Code and data are available on the project webpage: <https://zju3dv.github.io/pvo/>.

## 1 Introduction

Understanding the scene’s motion, geometry, and panoptic segmentation plays a crucial role in computer vision and robotics, with applications ranging from autonomous driving to augmented reality. In this work, we take a step toward solving this problem with monocular videos to achieve more comprehensive modeling of the scene.

This problem can be divided into two sub-tasks, namely visual odometry (VO) and video panoptic segmentation (VPS). In particular, VO [8, 9, 30] takes monocular video as input and estimates the camera pose for each frame. Some dynamic SLAM systems [1, 37] or visual semantic odometry (VSO) [19] propose to explicitly filter out potentially moving objects like pedestrians or vehicles using networks such as Mask R-CNN [11]. However, these approaches commonly ignore useful information for tracking, such as a stationary vehicle. While VPS [13, 36, 41] focuses on tracking individual instances in the scene given some initial panoptic segmentation results, which does not explicitly distinguish whether the object is moving or not. Notice that dynamic objects in the scene make both tasks challenging, existing approaches broadly solve these two tasks independently

---

\*Both authors contributed equally to this research.

†Corresponding author.

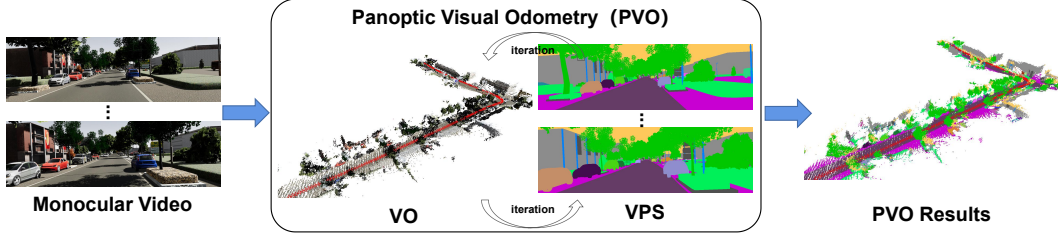


Figure 1: **Panoptic Visual Odometry** takes a monocular video as input and outputs the panoptic 3D map while simultaneously localizes the camera itself with respect to the map.

without recognizing their relevance. Some methods [5, 3, 17, 15] train motion-semantics networks in a multi-task manner, using loss functions that may contradict each other, which may drop the performance.

To address these problems, we propose a novel panoptic visual odometry (PVO) framework that tightly couples these two tasks using a unified view to model the scene comprehensively. Noticing that VPS can help adjust VO’s weight with panoptic segmentation information and VO can help track and fuse panoptic segmentation from 2D to 3D, we introduce a recurrent iterative optimization strategy, inspired by the seminal Expectation-Maximization algorithm [21], to make these two tasks mutually beneficial.

Our PVO consists of three modules, an image panoptic segmentation module, a Panoptic-Enhanced VO module and a VO-Enhanced VPS module. Specifically, the panoptic segmentation module takes a single image as input and outputs the image panoptic segmentation result, which is then fed into the Panoptic-Enhanced VO module as initialization. Note that although we choose PanopticFPN [16], any segmentation models can be used in the panoptic segmentation module. In the Panoptic-Enhanced VO module, we propose a panoptic update module to filter out the interference of dynamic objects and thus improve the accuracy of pose estimation in the dynamic scene, detailed in Sec 3.2. In the VO-Enhanced VPS module, we introduce an online fusion mechanism to align the multi-resolution features of the current frame to the adjacent frames using the pose, depth, and optical flow. This online fusion mechanism can effectively solve the problem of multiple objects occlusion, detailed in Sec 3.3. Experiments show that the recurrent iterative optimization strategy improves the performance of both VO and VPS. Overall, our contributions are summarised as four-fold.

- We present a novel Panoptic Visual Odometry (PVO) framework, which can unify VO and VPS tasks to model the scene comprehensively.
- We introduce a panoptic update module into the Panoptic-Enhanced VO module to improve the pose estimation.
- We propose an online fusion mechanism in the VO-Enhanced VPS module, which helps to improve the panoptic segmentation.
- Extensive experiments demonstrate that the proposed PVO with recurrent iterative optimization is superior to state-of-the-art methods in both visual odometry and video panoptic segmentation tasks.

## 2 Related Work

**Video Panoptic Segmentation.** VPS aims to generate consistent panoptic segmentation and track the instances to all pixels across video frames. A pioneer work, VPSNet [13] defines this novel task and proposes an instance-level tracking-based approach. SiamTrack [36] extends VPSNet by proposing a pixel-tube matching loss and a contrast loss to improve the discriminative power of instance embedding. VIP-Deeplab [24] presents a depth-aware VPS network by introducing additional depth information. While STEP [35] proposes to segment and track every pixel for video panoptic segmentation, HybridTracker [41] tracks instances from two perspectives — the feature space and the spatial location.

Different from existing methods, we introduce a VO-Enhanced VPS module, which exploits the camera pose, depth and optical flow estimated from VO to handle occlusion. Our online fusion

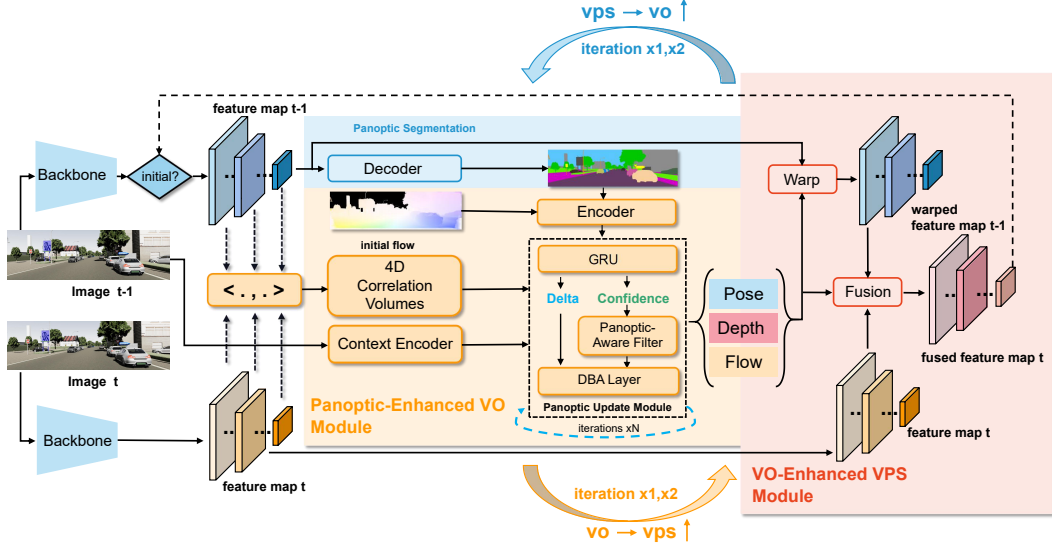


Figure 2: **Panoptic Visual Odometry Architecture.** Our method consists of three modules, namely, an image panoptic segmentation module for system initialization (blue), a Panoptic-Enhanced VO module (orange), and a VO-Enhanced VPS module (red). The last two modules contribute to each other in a recurrent iterative manner.

mechanism can simultaneously track and fuse information from the current frame to the adjacent frames.

**SLAM and Visual Odometry.** A complete SLAM system simultaneously performs self-localization and map construction. A VO, which focuses on pose estimation usually serves as the front-end in a SLAM system. Modern SLAM systems roughly fall into two categories, geometric-based methods [7, 22, 9, 6], and learning-based methods [44, 29, 31, 34]. With supervised-learning-based methods achieving promising performance, lots of attention has also been paid to explore unsupervised-learning-based VO methods. Though lots of works have been proposed [42, 43, 25], the performance is not as good as the supervised ones. To improve the performance, multi-task learning with auxiliary tasks such as depth [40] and optical flow [45] have been introduced into unsupervised-learning-based VO methods. More recently, TartanVO [32] proposes to build a generalizable learning-based VO and tests the system on a challenging SLAM dataset — TartanAir [33]. Also focusing on generalizability, DROID-SLAM [28] is proposed with recurrent iterative updates of camera pose and pixel-wise depth through a dense bundle adjustment layer and demonstrates superior performance.

Our panoptic-enhanced VO is built on DROID-SLAM with an additional panoptic update module, making it possible to better understand of scene geometry and semantics. Hence it demonstrates robust performance in dynamic scenes. Unlike other multi-task end-to-end models [15], our PVO has a recurrent iterative optimization strategy which prevents the sub-tasks from jeopardizing each other.

### 3 Method

Panoptic Visual Odometry (PVO) takes a monocular video as input and outputs the panoptic 3D map while simultaneously localising the camera itself with respect to the map, shown in Fig. 1. Fig. 2 shows an overview of our PVO method, which consists of three main modules: an image panoptic segmentation module, a Panoptic-Enhanced VO module, and a VO-Enhanced VPS module. The VO module aims at performing camera pose, depth, and optical flow estimations, while the VPS module outputs the corresponding video panoptic segmentation results with the given video. The last two modules contribute to each other in a recurrent interactive manner. The insight of PVO is to unify both VO and VPS tasks to build a comprehensive understanding of scene, thus improving the performance in both tasks.

### 3.1 Image Panoptic Segmentation

Image panoptic segmentation takes a single image as input, and outputs the panoptic segmentation of the image, which combines semantic segmentation and instance segmentation to model the instances of the image comprehensively. The output result is later used to first initialize video panoptic segmentation and then fed into the Panoptic-Enhanced VO module mentioned below. In our experiments, if not specifically indicated, we use the widely-used image panoptic segmentation network, PanopticFPN [16]. PanopticFPN first uses the backbone of ResNet50 as  $f_{\theta_e}$  with weight  $\theta_e$  to extract multi-scale features of image  $I_t$ :

$$\mathbf{z}_t = f_{\theta_e}(I_t) \quad (1)$$

and then outputs the panoptic segmentation results using a decoder  $g_{\theta_d}$  with weights  $\theta_d$ , consisting of semantic segmentation and instance segmentation. The panoptic segmentation results of each pixel  $\mathbf{p}$  are:

$$P_s(\mathbf{p}|\mathbf{z}_t) = g_{\theta_d}(\mathbf{p}, \mathbf{z}_t). \quad (2)$$

The multi-scale features which are fed into the decoder are updated over time. In the beginning, the multi-scale features generated by the encoder are directly fed into the decoder. In the later timesteps, these multi-scale features are updated with the online feature fusion module before being fed into the decoder, details about the fusion process are discussed in Sec 3.3.

### 3.2 Panoptic-Enhanced VO Module

In visual odometry, where dynamic scenes are ubiquitous, it is crucial to filter out the interference of dynamic objects. The front-end of DROID-SLAM [28] optimizes the residuals of camera pose and depth by iteratively optimizing optical flow residual with confidence. More details are illustrated in the supp. material. It does not consider that most backgrounds are static, and foreground objects may be dynamic. The insight of the Panoptic-Enhanced VO module is to assist in obtaining better confidence estimation, shown in Fig. 5, by incorporating information from the panoptic segmentation. Thus, Panoptic-Enhanced VO can get more accurate camera poses. As shown in Fig. 3, our Panoptic-Enhanced VO module, inherited from the front-end VO module of DROID-SLAM [28], combines the information from panoptic segmentation with optical flow information through an optical flow encoder to obtain a panoptic-aware optical flow representation.

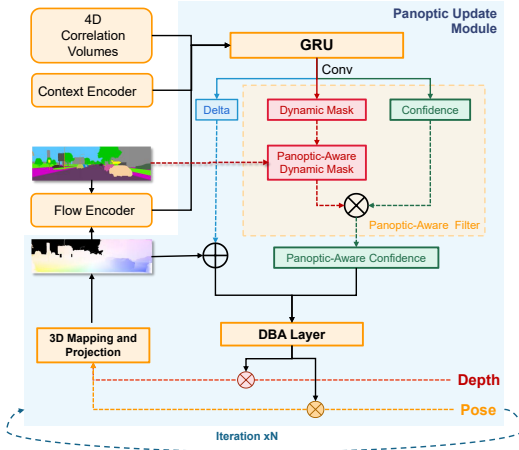


Figure 3: Panoptic-Enhanced VO Module.

**Panoptic Update Module.** The panoptic-aware flow representation and the 4D correlation volumes established from the two frames and the features acquired by the context encoder are fed to the GRU as intermediate variables, and then the three convolutional layers output a dynamic mask  $\mathbf{M}_{dij} \in \mathbb{R}^{H \times W \times 2}$ , a correlation confidence map  $\mathbf{w}_{ij} \in \mathbb{R}^{H \times W \times 2}$  and a dense optical flow delta  $\mathbf{r}_{ij} \in \mathbb{R}^{H \times W \times 2}$ , respectively. We can adjust the dynamic mask to the panoptic-aware dynamic mask given the initialized panoptic segmentation. For understanding, we leave the notation unchanged. Especially, the stuff segmentation will be set as static, while the foreground objects with high dynamic probability will be set as dynamic. The confidence and panoptic-aware dynamic mask are passed through a panoptic-aware filter module to obtain the panoptic-aware confidence:

$$\mathbf{w}_{p_{ij}} = \text{sigmoid}(\mathbf{w}_{ij} + (1 - \mathbf{M}_{dij}) \cdot \eta) \quad (3)$$

where  $\eta$  is set as 10. The obtained flow delta adding the original optical flow is fed to the dense bundle adjustment (DBA) layer to optimize the depth and pose residual.

The panoptic update module is iteratively optimized  $N$  times until convergence. Following DROID-SLAM [28], the pose residuals are applied to the current pose through retraction on the SE3 manifold,

while the depth and the dynamic mask residuals are added to the current depth and dynamic mask respectively:

$$\mathbf{G}^{(k+1)} = \text{Exp}(\Delta \xi^{(k)}) \circ \mathbf{G}^{(k)}, \quad \Theta^{(k+1)} = \Delta \Theta^{(k)} + \Theta^{(k)}, \quad \Theta \in \{\mathbf{d}, \mathbf{M}_d\}. \quad (4)$$

**Correspondence.** We first use the current pose and depth estimates at each iteration to search for the correspondence. Given a grid of pixel coordinates,  $\mathbf{p}_i \in \mathbb{R}^{H \times W \times 2}$  in frame  $i$ , we compute the dense correspondence field  $\mathbf{p}_{ij}$

$$\mathbf{p}_{ij} = \Pi_c(\mathbf{G}_{ij} \circ \Pi_c^{-1}(\mathbf{p}_i, \mathbf{d}_i)), \quad \mathbf{p}_{ij} \in \mathbb{R}^{H \times W \times 2}, \quad \mathbf{G}_{ij} = \mathbf{G}_j \circ \mathbf{G}_i^{-1}, \quad (5)$$

for each edge  $(i, j) \in \mathcal{E}$  in the frame graph, referred to DROID-SLAM [28]. Here  $\Pi_c$  is the camera model that maps a set of 3D points onto the image, and  $\Pi_c^{-1}$  is the inverse projection function that maps the inverse depth map  $\mathbf{d}$  and the coordinate grid  $\mathbf{p}_i$  to the 3D point cloud.  $\mathbf{p}_{ij}$  represents the coordinates of pixel  $\mathbf{p}_i$  mapped to  $j$  frames using the current pose and depth estimates.

**DBA Layer.** The dense bundle adjustment layer (DBA) maps a set of stream revisions to a set of pose and pixel depth updates. The cost function on the whole frame diagram is:

$$\mathbf{E}(\mathbf{G}', \mathbf{d}') = \sum_{(i,j) \in \mathcal{E}} \|\mathbf{p}_{ij}^* - \Pi_c(\mathbf{G}_{ij}' \circ \Pi_c^{-1}(\mathbf{p}_i, \mathbf{d}_i'))\|_{\Sigma_{ij}}^2, \quad (6)$$

$$\Sigma_{ij} = \text{diag } \mathbf{w}_{\mathbf{p}_{ij}}, \quad (7)$$

We use a local parameterization to linearize the Equation 6 and use the Gauss-Newton algorithm to solve for the update  $(\Delta \xi, \Delta \Theta)$ .

### 3.3 VO-Enhanced VPS Module

Video panoptic segmentation aims to obtain panoptic segmentation results for each frame and maintain the segmentation’s consistency between frames. To improve the segmentation accuracy and tracking accuracy, some methods such as FuseTrack [13] try to use optical flow information to fuse features and track them according to the similarity of features. These methods only come from a 2D perspective that may encounter occlusion or violent motion. We live in a 3D world where additional depth information can be used to model the scene better. Our VO-Enhanced VPS module is based on this understanding and can better solve the mentioned problems.

Fig. 4 shows our VO-Enhanced VPS module, which obtains the warped feature by warping the feature of the previous frame  $t-1$  to the current frame  $t$ , using the depth, pose, and optical flow information obtained from visual odometry. An online fusion module will fuse the features of the current frame  $t$  and the warped features to obtain the fused features. On the one hand, the fused feature will be applied to the next iteration of the Panoptic-Enhanced VO module. On the other hand, it will be fed to the decoder network to obtain the panoptic segmentation results. To keep the consistency of the video segmentation, we firstly feed the warped features (containing geometric motion information) into the decoder to obtain the warped segmentation results. Then a simple IoU-match module is used to obtain a consistent panoptic segmentation.

**VO-Aware Online Fusion.** The feature fusion network first concatenates the two features  $\mathbf{z}_{t-1}$  and  $\mathbf{z}_t$ , and then passes through a convolutional layer with ReLU activations to obtain the fused features  $\hat{\mathbf{z}}_t$ . Inspired by NeuralBlox [20], we propose two loss functions for supervision to ensure that online feature fusion can be effective (see Tab. 7).

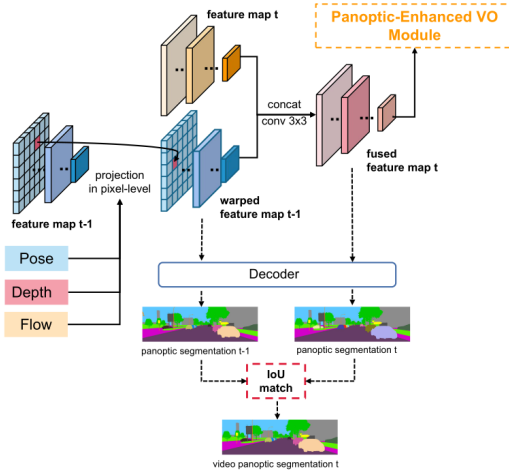


Figure 4: VO-Enhanced VPS Module.



**Feature Alignment Loss [20]:** We employ a feature alignment loss to minimize the distance between  $\mathbf{z}_t^*$  and  $\hat{\mathbf{z}}_t$  in latent space:

$$\mathcal{L}_{fea} = \|\mathbf{z}_t^* - \hat{\mathbf{z}}_t\|_1 \quad (8)$$

where  $\mathbf{z}_t^*$  denotes the average feature of the same pixel point from different images all warping to the same image.

**Segmentation Consistent Loss:** Additionally, we add a segmentation loss that minimizes the logit differences of query pixels  $\mathbf{p}$  decoded using  $\mathbf{z}_t^*$  and  $\hat{\mathbf{z}}_t$ :

$$\mathcal{L}_{seg} = \sum_{\mathbf{p} \in \mathbb{P}} \|g_{\theta_d}(\mathbf{p}, \mathbf{z}_t^*) - g_{\theta_d}(\mathbf{p}, \hat{\mathbf{z}}_t)\|_1 \quad (9)$$

### 3.4 Recurrent Iterative Optimization

We can optimize our proposed Panoptic-Enhanced VO module and VO-Enhanced VPS module in a recurrent iterative manner until convergence, which is inspired by the EM algorithm. Experimentally, it takes only two iterations for the loop to converge. Tab. 6 and Tab. 7 demonstrates that recurrent iterative optimization can boost the performance of the VPS and VO module.

### 3.5 Implementation Details

This section will elaborate on the details of our implementation, which focuses on the training details. PVO is implemented in PyTorch and consists of three main modules: image panoptic segmentation, Panoptic-Enhanced VO module, and VO-Enhanced VPS module. We use three stages to train our network. Image panoptic segmentation is now trained on datasets such as VKITTI2 [2] as initialization. We adopt multi-scale inference scaling equal to 0.5, 0.625, 0.75, 0.875, 1 for  $375 \times 1242$  VKITTI2. We optimize the network with an initial rate of  $1e-4$  on 2 GeForce RTX 3090 GPUs, where each mini-batch has eight images. The optimizer is SGD with weight decay  $1e-4$  and momentum 0.9. The training of the Panoptic-Enhanced VO module follows DROID-SLAM [28], except that it additionally feeds the segmented ground-truth panoptic segmentation results. Specifically, we trained this module on the VKITTI2 dataset with 2 RTX-3090 GPUs for 80,000 steps, which took about two days. When training the VO-enhanced video panoptic segmentation module, we use the ground-truth depth, optical flow, and pose information as geometric priors to align the features, fix the backbone of the trained single-image panoptic segmentation, and train only the fusion module. We optimize the network with an initial learning rate of  $1e-5$  and 1 GeForce RTX 3090 GPU, where each batch has eight images. When the fusion network has largely converged, we add a segmentation consistency loss function to refine our VPS module further.

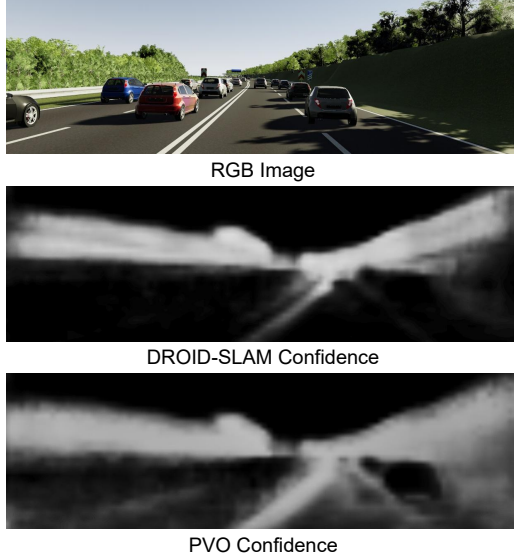


Figure 5: **Panoptic-Aware Confidence.** We visualize the confidence of our PVO vs. DROID-SLAM. We can see that with panoptic information, the panoptic weights can better remove the dynamic interference and keep the static features for solving the camera pose. The black color indicates that the confidence tends to be close to 0.

## 4 Experiments

For visual odometry, we conduct experiments on three datasets with dynamic scenes: VKITTI2, KITTI, and TUM RGBD dynamic sequences, to evaluate the accuracy of the camera trajectory, primarily using Absolute Trajectory Error. For video panoptic segmentation, we evaluate the VPQ metric used in FuseTrack [14] on Cityscapes and VIPER datasets. We also perform ablation studies to analyze the design of our framework.

#### 4.1 Visual Odometry

Monocular	vkitti01	vkitti02	vkitti06	vkitti18	vkitti20	Avg
DROID-SLAM [28]	1.091	<b>0.025</b>	0.113	1.156	8.285	2.134
Ours (VPS->VO w/o filter)	0.384	0.061	0.116	0.936	5.375	1.374
Ours (VPS->VO)	0.374	0.057	0.113	0.960	3.487	0.998
Ours (VPS->VO x2)	0.371	0.057	0.113	0.954	3.135	0.926
Ours (VPS->VO x3)	<b>0.369</b>	0.055	<b>0.113</b>	<b>0.822</b>	<b>3.079</b>	<b>0.888</b>
DROID-SLAM's runtime (FPS)	5.73	12.67	19.96	7.08	10.20	11.13
Ours' runtime (FPS)	4.45	9.69	14.52	6.22	8.10	8.60

Table 1: **Panoptic-Enhanced VO Module Results on Virtual KITTI2 Dataset.** Panoptic-Enhanced VO module outperforms DROID-SLAM on most of the highly dynamic VKITTI2 datasets, and the accuracy of the pose estimation is significantly improved and slightly slowed down after recurrent iterative optimization.

**VKITTI2.** Virtual KITTI dataset [2] which consists of 5 sequence clones from the KITTI tracking benchmark, provides RGB, depth, class segmentation, instance segmentation, camera pose, flow, and scene flow data for each sequence. In the ablation study, we use the dataset of clone as the training set, 15-degree rotation as the validation set, and 30-degree rotation as the test set. As shown in Tab. 1 and Fig. 6, our PVO outperforms DROID-SLAM by a large margin except for the vkitti02 sequence.

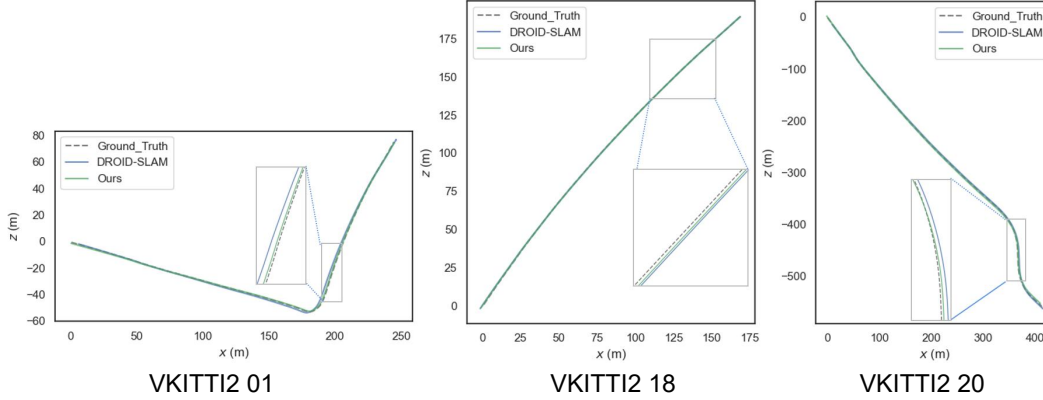


Figure 6: **Trajectory Comparison.** Compared our methods with DROID-SLAM on 01, 18, and 20 sequences of VKITTI2. In these sequences with dynamic scenes, our method performs better than DROID-SLAM, having better trajectory estimation results.

**KITTI.** KITTI [10] is a dataset capturing real-world traffic situations and ranging from free-ways over rural areas to inner-city scenes with many static and dynamic objects. We use KITTI's 09 and 10 sequences to verify the accuracy of our system in a dynamic environment. In the visual odometry task, we applied the PVO model trained on the VKITTI2 [2] dataset to the KITTI [10] dataset. Compared with DROID-SLAM, we achieve nearly half of the pose estimation error in DROID-SLAM, shown in Fig. 7, which demonstrates good generalization ability of PVO. The reason is that the VKITTI2 and KITTI scenarios are generally similar.

**TUM-RGBD.** The RGBD dataset consists of indoor scenes captured with handheld camera. We

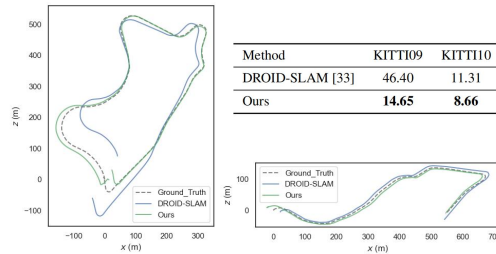


Figure 7: **Generalization results on the KITTI benchmark.** The trajectories of ours vs DROID-SLAM trained on VKITTI2 datasets. Our method is largely superior to DROID-SLAM [28]. Left: KITTI09, Right: KITTI10.

Sequences		Trans. RMSE of trajectory alignment [m]				
		DVO SLAM [12]	ORB-SLAM2 [23]	PointCorr [4]	DROID-SLAM [28]	Ours
slightly dynamic	fr2/desk-person	0.104	<b>0.006</b>	0.008	0.017	0.013
	fr3/sitting-static	0.012	0.008	0.010	0.007	<b>0.006</b>
	fr3/sitting-xyz	0.242	0.010	<b>0.009</b>	0.016	0.014
	fr3/sitting-rpy	0.176	0.025	<b>0.023</b>	0.029	0.027
	fr3/sitting-halfsphere	0.220	0.025	0.024	0.026	<b>0.022</b>
highly dynamic	fr3/walking-static	0.752	0.408	0.011	0.016	<b>0.007</b>
	fr3/walking-xyz	1.383	0.722	0.087	0.019	<b>0.018</b>
	fr3/walking-rpy	1.292	0.805	0.161	0.059	<b>0.056</b>
	fr3/walking-halfsphere	1.014	0.723	<b>0.035</b>	0.312	0.221

Table 2: **Comparison of the absolute trajectory error (ATE) on the TUM benchmark.** The best results are shown in bold. PVO achieves competitive and even best performance.

Methods on Cityscapes-VPS val	Temporal window size				VPQ	FPS
	k = 0	k = 5	k = 10	k = 15		
VPSNet-Track	63.1 / 56.4 / 68.0	56.1 / 44.1 / 64.9	53.1 / 39.0 / 63.4	51.3 / 35.4 / 62.9	55.9 / 43.7 / 64.8	4.5
VPSNet-FuseTrack	64.5 / 58.1 / 69.1	57.4 / 45.2 / 66.4	54.1 / 39.5 / 64.7	52.2 / 36.0 / 64.0	57.2 / 44.7 / 66.6	1.3
SiamTrack	64.6 / 58.3 / 69.1	57.6 / 45.6 / 66.6	54.2 / 39.2 / 65.2	52.7 / 36.7 / 64.6	57.3 / 44.7 / 66.4	4.5
PanopticFCN [18] + Ours	<b>65.6</b> / 60.0 / 69.7	<b>57.8</b> / 45.7 / 66.6	54.3 / 39.5 / 65.1	52.1 / 35.4 / 64.3	<b>57.5</b> / 45.1 / 66.4	5.1
VPSNet-FuseTrack + Ours	65.0 / 59.0 / 69.4	57.6 / 45.0 / 66.7	<b>54.4</b> / 39.1 / 65.6	<b>52.8</b> / 35.8 / 65.2	<b>57.5</b> / 44.7 / 66.7	1.1

Table 3: **Comparison of video panoptic segmentation results on Cityscapes-VPS validation dataset with our VO-Enhanced VPS module variants.** Each cell contains VPQ / VPQ<sup>Th</sup> / VPQ<sup>St</sup> scores. The best results are highlighted in boldface. Our methods generally outperform VPSNet-FuseTrack [14] and SiamTrack [36].

choose the dynamic sequences of TUM RGBD dataset to show the effectiveness of our methods. Table. 2 demonstrates that our methods perform better on all datasets, compared with DROID-SLAM. We achieve the best results on 5 dataset out of 9 datasets. Note that PointCorr [4] is a state-of-the-art RGB-D SLAM using Point Correlation, while ours only used monocular RGB video.

## 4.2 Video Panoptic Segmentation

We have selected 3 instance-based video panoptic segmentation methods as comparison, including VPSNet-Track, VPSNet-FuseTrack [14] and SiamTrack [36]. VPSNet-Track is a basic video panoptic segmentation model which adds MaskTrack head [39] on top of the image panoptic segmentation model, UPSNet [38]. VPSNet-FuseTrack Based on VPSNet-Track, additionally supports temporal feature aggregation and attentional space-time feature fusion. While SiamTrack finetunes VPSNet-Track with the pixel-tube matching loss and the contrast loss is only slightly better than VPSNet-FuseTrack. We mainly compare with VPSNet-FuseTrack as SiamTrack’s source code is not publicly available. The VPQ results are borrowed from SiamTrack [36].

**Cityscapes.** We follow VPS [14]’s public train/val/ test split. Each video consists of 30 consecutive frames, with every five frames paired with the ground truth annotations. All 30 frames of each video are predicted, and only six frames with the ground truth are evaluated. Tab. 3 summarizes Video Panoptic Segmentation (VPQ) results of all the methods on the Cityscapes-VPS val dataset. We observe that our method with PanopticFCN [18] outperforms the state-of-the-art method, achieving **+1.6% VPQ** higher than VPSNet-Track for val dataset. Fig. 11 demonstrates our method can keep consistent video segmentation, compared with VPSNet-FuseTrack [13].

Methods on VIPER	Temporal window size				VPQ	FPS
	k = 0	k = 5	k = 10	k = 15		
VPSNet-Track	48.1 / 38.0 / 57.1	49.3 / 45.6 / 53.7	45.9 / 37.9 / 52.7	43.2 / 33.6 / 51.6	46.6 / 38.8 / 53.8	5.1
VPSNet-FuseTrack	49.8 / 40.3 / 57.7	51.6 / 49.0 / 53.8	47.2 / 40.4 / 52.8	45.1 / 36.5 / 52.3	48.4 / 41.6 / 53.2	1.6
SiamTrack	51.1 / 42.3 / 58.5	<b>53.4</b> / 51.9 / 54.6	49.2 / 44.1 / 53.5	47.2 / 40.3 / 52.9	50.2 / 44.7 / 55.0	5.1
PanopticFCN + Ours	<b>54.6</b> / 50.3 / 57.9	51.7 / 44.5 / 57.3	<b>50.5</b> / 41.8 / 57.2	<b>49.1</b> / 38.9 / 56.9	<b>51.5</b> / 43.9 / 57.3	3.6

Table 4: **Comparison of video panoptic segmentation results on VIPER with our VO-Enhance VPS variants.** Each cell contains VPQ / VPQ<sup>Th</sup> / VPQ<sup>St</sup> scores. The best results are highlighted in boldface. Our methods generally outperform VPSNet-FuseTrack [14] and SiamTrack [36].



Methods on <b>VKITTI2</b>	Temporal window size				VPQ
	k = 0	k = 5	k = 10	k = 15	
VPS baseline	58.24 / 60.11 / 57.93	55.50 / 53.78 / 56.28	54.13 / 50.29 / 55.53	53.65 / 48.53 / 55.46	54.90 / 51.95 / 56.05
Ours (VO->VPS + w/o fusion)	58.24 / 60.11 / 57.93	55.67 / 54.44 / 56.28	54.29 / 50.91 / 55.53	53.83 / 49.22 / 55.46	55.04 / 52.48 / 56.05
Ours (VO->VPS + w/fusion + w/o fea loss)	58.51 / 64.07 / 56.97	55.62 / 58.53 / 54.86	54.29 / 55.15 / 54.13	53.94 / 53.40 / 54.19	55.14 / 56.62 / 54.81
Ours (VO->VPS + w/fusion + w/o seg loss)	58.73 / 65.05 / 56.95	55.83 / 59.34 / 54.89	54.51 / 56.01 / 54.15	54.15 / 54.26 / 54.19	55.37 / 57.49 / 54.82
VPS baseline + w/fusion	59.16 / 67.00 / 56.91	56.27 / 60.98 / 54.96	54.96 / 57.74 / 54.18	54.58 / 55.97 / 54.19	55.81 / 59.23 / 54.85
Ours (VO->VPS)	59.18 / 67.00 / 56.94	56.25 / 61.00 / 54.93	54.94 / 57.77 / 54.15	54.57 / 56.01 / 54.17	55.80 / 59.25 / 54.83
Ours (VO->VPS) x2	<b>59.18</b> / 67.00 / 56.94	<b>56.42</b> / 61.67 / 54.93	<b>55.10</b> / 58.40 / 54.15	<b>54.84</b> / 56.67 / 54.17	<b>55.94</b> / 59.77 / 54.83

Table 5: **Ablation Study of our VO-Enhanced VPS module variants on VKITTI2 dataset.** Comparison of video panoptic segmentation results. Each cell contains VPQ / VPQ<sup>Th</sup> / VPQ<sup>St</sup> scores. The best results are highlighted in boldface. Our method performs better.

**VIPER.** VIPER is a video panoptic segmentation benchmark with high quantity and quality of the panoptic video annotations. Following VPS[14], we follow the public train/val/split. For evaluation, we choose 10 validation videos from the day scenario and use the first 60 frames of each video: 600 images. Table 4 summarizes the VPQ results of all the methods on VIPER datasets, and we observe a consistent tendency. Compared with VPSNet-FuseTrack, our method with PanopticFCN achieves much higher scores (**51.5VPQ** vs. 48.4 VPQ).

### 4.3 Ablation Study

**VPS-Enhanced VO Module.** In the Panoptic-Enhanced VO module, we use DROID-SLAM [28] as our baseline. (VPS->VO) means the panoptic information prior was added to enhance the VO baseline. (VPS->VO x2) means that we can recurrent iteratively optimize the VO module twice. (VPS->VO x3) means recurrent iteratively optimization on the VO module 3 times. As shown in Tab. 6 and Fig. 5, the panoptic information can help improve the accuracy of DROID-SLAM on most of the highly dynamic VKITTI2 datasets. The recurrent iterative optimization can further improve the results.

**VO Enhanced VPS Module.** To evaluate whether VO helps VPS, the VPQ metric [14] is adopted to evaluate the spatial-temporal consistency between the predicted and ground truth video panoptic segmentation. We first use PanopticFPN [16] to get the panoptic segmentation results for each frame, and then use the optical flow information from RAFT [26] for inter-frame tracking. This is set as VPS baseline. (VPS baseline + w/fusion) means we additionally fuse the feature with the flow estimation. (VO->VPS + w/o fusion) means that we use additional depth, pose, and other information on top of the baseline. (VO->VPS) means we additionally fuse the feature. (VO->VPS x2) means that we use the recurrent iterative optimization module to enhance the VPS results further. As shown in Tab. 7 and Fig.8, the VO-Enhanced VPS module is effective in improving segmentation accuracy and tracking consistency.

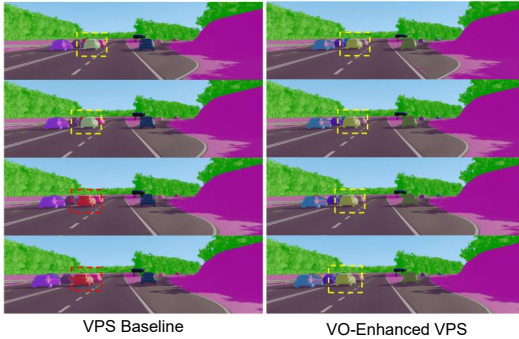


Figure 8: **Comparison results of our VO-Enhanced VPS module with VPS baseline on VKITTI2 dataset.** Our method keeps the consistent video segmentation. Different colors in the figure indicate tracking failure.

**Online Fusion in VO-Enhanced VPS Module.** To validate the effectiveness of the proposed Feature Alignment Loss (fea loss) and Segmentation Consistent Loss (seg loss), the methods are followed: (VO->VPS + w/fusion + w/o fea loss) means that we train the online fusion module without Feature Alignment Loss. (VO->VPS + w/fusion + w/o seg loss) means that we train the online fusion module without Segmentation Consistent Loss. Tab. 7 demonstrates the effectiveness of these two loss function.

## 5 Conclusion

We present a novel panoptic visual odometry method, which models the visual odometry (VO) task for estimating scene motion and the video panoptic segmentation (VPS) task for perceiving the scene in a unified view, enabling the two tasks to facilitate each other. The panoptic update module can help improve the pose estimation, while the online fusion module helps improve the panoptic segmentation. Extensive experiments demonstrate that panoptic visual odometry outperforms state-of-the-art methods in visual odometry and video panoptic segmentation tasks.

## 6 Acknowledgements

This work was partially supported by NSF of China (No. 61932003) and ZJU-SenseTime Joint Lab of 3D Vision.

## References

- [1] B. Bescos, J. M. Fácil, J. Civera, and J. Neira. Dynaslam: Tracking, mapping, and inpainting in dynamic scenes. *IEEE Robotics and Automation Letters*, 3(4):4076–4083, 2018.
- [2] Y. Cabon, N. Murray, and M. Humenberger. Virtual kitti 2. *arXiv preprint arXiv:2001.10773*, 2020.
- [3] J. Cheng, Y.-H. Tsai, S. Wang, and M.-H. Yang. Segflow: Joint learning for video object segmentation and optical flow. In *Proceedings of the IEEE international conference on computer vision*, pages 686–695, 2017.
- [4] W. Dai, Y. Zhang, P. Li, Z. Fang, and S. Scherer. Rgb-d slam in dynamic environments using point correlations. *IEEE Transactions on Pattern Analysis and Machine Intelligence*, 44(1):373–389, 2020.
- [5] M. Ding, Z. Wang, B. Zhou, J. Shi, Z. Lu, and P. Luo. Every frame counts: Joint learning of video segmentation and optical flow. In *Proceedings of the AAAI Conference on Artificial Intelligence*, volume 34, pages 10713–10720, 2020.
- [6] J. Engel, V. Koltun, and D. Cremers. Direct sparse odometry. *IEEE transactions on pattern analysis and machine intelligence*, 40(3):611–625, 2017.
- [7] J. Engel, T. Schops, and D. Cremers. LSD-SLAM: Large-scale direct monocular slam. In *ECCV*, 2014.
- [8] J. Engel, J. Sturm, and D. Cremers. Semi-dense visual odometry for a monocular camera. In *ICCV*, pages 1449–1456, 2013.
- [9] C. Forster, M. Pizzoli, and D. Scaramuzza. Svo: Fast semi-direct monocular visual odometry. In *ICRA*, pages 15–22. IEEE, 2014.
- [10] A. Geiger, P. Lenz, C. Stiller, and R. Urtasun. Vision meets robotics: The kitti dataset. *The International Journal of Robotics Research*, 32(11):1231–1237, 2013.
- [11] K. He, G. Gkioxari, P. Dollár, and R. Girshick. Mask r-cnn. In *Proceedings of the IEEE International Conference on Computer Vision (ICCV)*, Oct 2017.
- [12] C. Kerl, J. Sturm, and D. Cremers. Robust odometry estimation for rgb-d cameras. In *2013 IEEE international conference on robotics and automation*, pages 3748–3754. IEEE, 2013.
- [13] D. Kim, S. Woo, J.-Y. Lee, and I. S. Kweon. Video panoptic segmentation. In *Proceedings of the IEEE/CVF Conference on Computer Vision and Pattern Recognition*, pages 9859–9868, 2020.
- [14] D. Kim, S. Woo, J.-Y. Lee, and I. S. Kweon. Video panoptic segmentation. In *Proceedings of the IEEE Conference on Computer Vision and Pattern Recognition*, 2020.
- [15] U.-H. Kim, S.-H. Kim, and J.-H. Kim. Simvodi: Simultaneous visual odometry, object detection, and instance segmentation, 2019.
- [16] A. Kirillov, R. Girshick, K. He, and P. Dollár. Panoptic feature pyramid networks. In *Proceedings of the IEEE/CVF Conference on Computer Vision and Pattern Recognition*, pages 6399–6408, 2019.
- [17] J. Li, J. Zhao, S. Song, and T. Feng. Unsupervised joint learning of depth, optical flow, ego-motion from video. *arXiv preprint arXiv:2105.14520*, 2021.
- [18] Y. Li, H. Zhao, X. Qi, L. Wang, Z. Li, J. Sun, and J. Jia. Fully convolutional networks for panoptic segmentation. In *IEEE Conference on Computer Vision and Pattern Recognition (CVPR)*, pages 214–223, 2021.
- [19] K.-N. Lianos, J. L. Schonberger, M. Pollefeys, and T. Sattler. Vso: Visual semantic odometry. In *Proceedings of the European conference on computer vision (ECCV)*, pages 234–250, 2018.
- [20] S. Lionar, L. Schmid, C. Cadena, R. Siegwart, and A. Cramariuc. Neuralblox: Real-time neural representation fusion for robust volumetric mapping. In *2021 International Conference on 3D Vision (3DV)*, pages 1279–1289. IEEE, 2021.
- [21] T. Moon. The expectation-maximization algorithm. *IEEE Signal Processing Magazine*, 13(6):47–60, 1996.
- [22] R. Mur-Artal, J. M. M. Montiel, and J. D. Tardos. Orb-slam: a versatile and accurate monocular slam system. *IEEE transactions on robotics*, 31(5):1147–1163, 2015.

- [23] R. Mur-Artal and J. D. Tardós. Orb-slam2: An open-source slam system for monocular, stereo, and rgb-d cameras. *IEEE Transactions on Robotics*, 33(5):1255–1262, 2017.
- [24] S. Qiao, Y. Zhu, H. Adam, A. Yuille, and L.-C. Chen. Vip-deeplab: Learning visual perception with depth-aware video panoptic segmentation. In *Proceedings of the IEEE/CVF Conference on Computer Vision and Pattern Recognition*, pages 3997–4008, 2021.
- [25] A. Ranjan, V. Jampani, L. Balles, K. Kim, D. Sun, J. Wulff, and M. J. Black. Competitive collaboration: Joint unsupervised learning of depth, camera motion, optical flow and motion segmentation. In *Proceedings of the IEEE/CVF Conference on Computer Vision and Pattern Recognition (CVPR)*, June 2019.
- [26] Z. Teed and J. Deng. Raft: Recurrent all-pairs field transforms for optical flow. In *European conference on computer vision*, pages 402–419. Springer, 2020.
- [27] Z. Teed and J. Deng. Raft: Recurrent all-pairs field transforms for optical flow. In *European Conference on Computer Vision*, pages 402–419. Springer, 2020.
- [28] Z. Teed and J. Deng. DROID-SLAM: Deep Visual SLAM for Monocular, Stereo, and RGB-D Cameras. *Advances in neural information processing systems*, 2021.
- [29] S. Vijayanarasimhan, S. Ricco, C. Schmidy, R. Sukthankar, and K. Fragkiadaki. Sfm-net: Learning of structure and motion from video. In *arXiv:1704.07804*, 2017.
- [30] S. Wang, R. Clark, H. Wen, and N. Trigoni. Deepvo: Towards end-to-end visual odometry with deep recurrent convolutional neural networks. In *2017 IEEE International Conference on Robotics and Automation (ICRA)*, pages 2043–2050. IEEE, 2017.
- [31] S. Wang, R. Clark, H. Wen, and N. Trigoni. End-to-end, sequence-to-sequence probabilistic visual odometry through deep neural networks. *The International Journal of Robotics Research*, 37(4-5):513–542, 2018.
- [32] W. Wang, Y. Hu, and S. Scherer. Tartanvo: A generalizable learning-based vo. 2020.
- [33] W. Wang, D. Zhu, X. Wang, Y. Hu, Y. Qiu, C. Wang, Y. Hu, A. Kapoor, and S. Scherer. Tartanair: A dataset to push the limits of visual slam. In *2020 IEEE/RSJ International Conference on Intelligent Robots and Systems (IROS)*, 2020.
- [34] X. Wang, D. Maturana, S. Yang, W. Wang, Q. Chen, and S. Scherer. Improving learning-based ego-motion estimation with homomorphism-based losses and drift correction. In *2019 IEEE/RSJ International Conference on Intelligent Robots and Systems (IROS)*, pages 970–976. IEEE, 2019.
- [35] M. Weber, J. Xie, M. Collins, Y. Zhu, P. Voigtlaender, H. Adam, B. Green, A. Geiger, B. Leibe, D. Cremers, et al. Step: Segmenting and tracking every pixel. *arXiv preprint arXiv:2102.11859*, 2021.
- [36] S. Woo, D. Kim, J.-Y. Lee, and I. S. Kweon. Learning to associate every segment for video panoptic segmentation. In *Proceedings of the IEEE/CVF Conference on Computer Vision and Pattern Recognition*, pages 2705–2714, 2021.
- [37] L. Xiao, J. Wang, X. Qiu, Z. Rong, and X. Zou. Dynamic-slam: Semantic monocular visual localization and mapping based on deep learning in dynamic environment. *Robotics and Autonomous Systems*, 117:1–16, 2019.
- [38] Y. Xiong, R. Liao, H. Zhao, R. Hu, M. Bai, E. Yumer, and R. Urtasun. Upsnet: A unified panoptic segmentation network. In *Proceedings of the IEEE/CVF Conference on Computer Vision and Pattern Recognition*, pages 8818–8826, 2019.
- [39] L. Yang, Y. Fan, and N. Xu. Video instance segmentation. In *Proceedings of the IEEE/CVF International Conference on Computer Vision*, pages 5188–5197, 2019.
- [40] N. Yang, L. v. Stumberg, R. Wang, and D. Cremers. D3vo: Deep depth, deep pose and deep uncertainty for monocular visual odometry. In *IEEE/CVF Conference on Computer Vision and Pattern Recognition (CVPR)*, June 2020.
- [41] W. Ye, X. Lan, G. Su, Z. Cui, H. Bao, and G. Zhang. Hybrid Tracker with Pixel and Instance for Video Panoptic Segmentation. In *arxiv*, 2022.
- [42] Z. Yin and J. Shi. Geonet: Unsupervised learning of dense depth, optical flow and camera pose. In *Proceedings of the IEEE Conference on Computer Vision and Pattern Recognition (CVPR)*, volume 2, 2018.
- [43] H. Zhan, R. Garg, C. S. Weerasekera, K. Li, H. Agarwal, and I. Reid. Unsupervised learning of monocular depth estimation and visual odometry with deep feature reconstruction. In *Proceedings of the IEEE Conference on Computer Vision and Pattern Recognition*, pages 340–349, 2018.
- [44] T. Zhou, M. Brown, N. Snavely, and D. G. Lowe. Unsupervised learning of depth and ego-motion from video. In *CVPR*, 2017.
- [45] Y. Zou, Z. Luo, and J.-B. Huang. Df-net: Unsupervised joint learning of depth and flow using cross-task consistency. In *Proceedings of the European Conference on Computer Vision (ECCV)*, September 2018.

## A Appendix

In this supplementary material, we will describe the difference between our method and existing methods, the preliminaries of DROID-SLAM, and more experiment results of our methods. We also show the video which demonstrates the qualitative results of our method.

### A.1 Illustration

Existing visual odometry can be broadly classified into two types: data-driven vo, which separates motion and semantic in two networks; and motion-semantic network such as SimVODIS [15], which optimizes motion and semantic information in a multi-task manner. Unlike existing approaches, Panoptic Visual Odometry (PVO) unifies visual odometry and video panoptic segmentation, allowing the two tasks to be mutually reinforcing by recurrent iterative optimization.

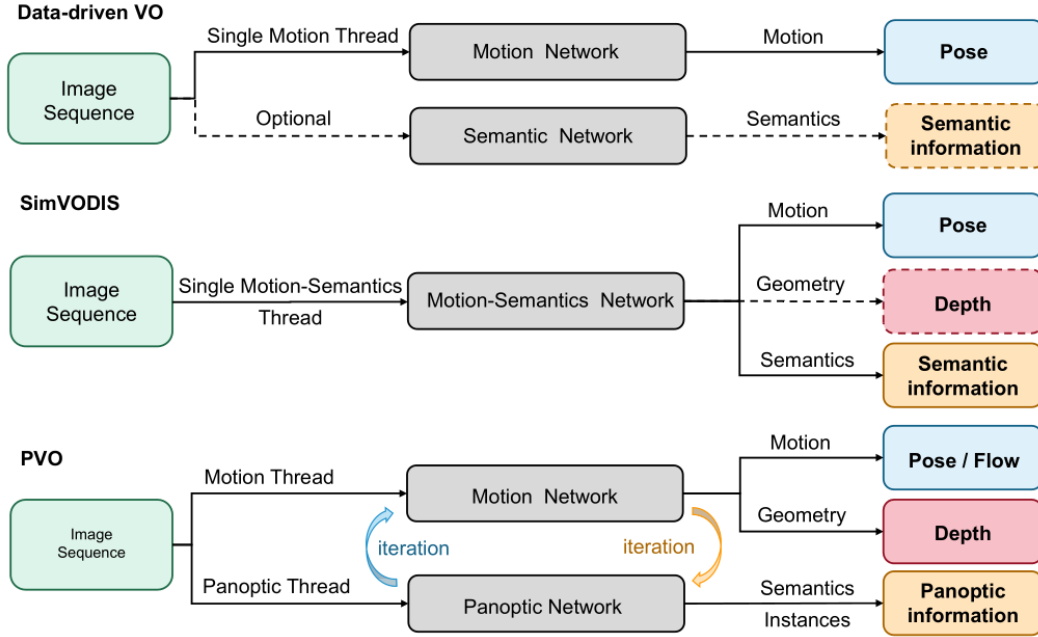


Figure 9: **Illustration.** Our PVO unifies visual odometry and video panoptic segmentation so that the two tasks can be mutually reinforced by iterative optimization. In contrast, methods such as SimVODIS [15] optimizes motion and semantic information in a multi-task manner.

### A.2 Preliminaries: DROID-SLAM

DROID-SLAM [28] is a deep learning based SLAM system, which consists of recurrent iterative updates of camera pose and pixelwise depth through a Dense Bundle Adjustment layer. It takes a video  $\{\mathbf{I}_t\}_{t=0}^N$  as input with two objectives: estimate the trajectory of the camera  $\mathbf{G}_t \in SE(3)$  and build a 3D map of the environment. For each image  $t$ , it maintain two unknown state variables: camera pose  $\mathbf{G}_t \in SE(3)$  and inverse depth  $\mathbf{d}_t \in \mathbb{R}_+^{H \times W}$ , which get iteratively updated during inference as new frames are processed.

DROID-SLAM [28] adopts a frame-graph  $(\mathcal{V}, \mathcal{E})$  to represent co-visibility between frames. An edge  $(i, j) \in \mathcal{E}$  means image  $\mathbf{I}_i$  and  $\mathbf{I}_j$  have overlapping fields of view which shared points. The frame graph is built dynamically during training and inference with the recomputed visibility.

#### A.2.1 Feature Extraction and Correlation

**Feature Extraction.** DROID-SLAM [28] borrowed the key components of RAFT[27] to extract the features. Each of the input images are processed by a feature extraction network, which consists of 6 residual blocks and 3 downsampling layers, producing dense feature maps at 1/8 the input image

resolution. It uses two separate networks: a feature network which is used to build the set of correlation volumes and a context network whose features are injected into the network during each application of the update operator.

**Correlation Pyramid.** For each edge in the frame graph,  $(i, j) \in \mathcal{E}$ , DROID-SLAM [28] computes a 4D correlation volume by taking the dot product between all-pairs of feature vectors in  $g_\theta(I_i)$  and  $g_\theta(I_j)$ :

$$C_{u_1 v_1 u_2 v_2}^{ij} = \langle g_\theta(I_i)_{u_1 v_1}, g_\theta(I_j)_{u_2 v_2} \rangle \quad (10)$$

then performs average pooling of the last two dimensions of the correlation volume following RAFT[27] to form a 4-level correlation pyramid.

**Correlation Lookup.** DROID-SLAM [28] defines a lookup operator which indexes the correlation volume using a grid with radius  $r$ ,  $L_r : \mathbb{R}^{H \times W \times H \times W} \times \mathbb{R}^{H \times W \times 2} \mapsto \mathbb{R}^{H \times W \times (r+1)^2}$ .

The lookup operator takes an  $H \times W$  grid of coordinates as input and values are retrieved from the correlation volume using bilinear interpolation. The operator is applied to each correlation volume in the pyramid and the final feature vector is computed by concatenating the results at each level.

### A.3 Experiments Results

#### A.3.1 Ablation Study of Panoptic-Enhanced VO Module

In our Panoptic-Enhanced VO module, unlike DROID-SLAM [28], we adjust the confidence by incorporating information from the panoptic segmentation. We can adjust the dynamic mask to the panoptic-aware dynamic mask given the initialized panoptic segmentation. For understanding, we leave the notation unchanged. Especially, the stuff segmentation will be set as static, while the foreground objects with high dynamic probability will be set as dynamic. Here, we find the dynamic threshold set as 0.5 may achieve the best results, shown in Tab. 6. The reason is that when the dynamic threshold is small, too many static pixel points may be removed, while the dynamic threshold is too large and small movements may be ignored. The confidence and panoptic-aware dynamic mask are passed through a panoptic-aware filter module to obtain the panoptic-aware confidence. As shown in Tab. 6, the panoptic-aware filter module can help improve the estimation of camera pose. Fig. 6 demonstrates that the panoptic information can help improve the accuracy of DROID-SLAM on most of the highly dynamic VKITTI2 datasets. Finally, we show the qualitative results of the panoptic 3D maps produced by our methods, shown in Fig. 10.

Monocular	vkitti01	vkitti02	vkitti06	vkitti18	vkitti20	Avg
DROID-SLAM	1.091	<b>0.025</b>	0.113	1.156	8.285	2.134
Ours (VPS->VO w/o filter)	0.384	0.061	0.116	0.936	5.375	1.374
Ours (VPS->VO)	0.374	0.057	0.113	0.960	3.487	0.998
Ours (VPS->VO x2)	0.371	0.057	0.113	0.954	3.135	0.926
Ours (VPS->VO x3)	<b>0.369</b>	0.055	0.113	<b>0.822</b>	<b>3.079</b>	<b>0.888</b>
(Ours x3) threshold=0.1	0.377	0.052	<b>0.112</b>	0.950	3.240	0.946
(Ours x3) threshold=0.3	0.374	0.054	0.113	0.946	3.107	0.919
(Ours x3) threshold=0.5	0.369	0.055	0.113	0.822	3.079	0.888
(Ours x3) threshold=0.7	0.384	0.059	0.114	0.863	22.993	4.883
(Ours x3) threshold=0.9	1.348	0.065	0.119	0.885	17.337	3.951

Table 6: **Ablation Study of Panoptic-Enhanced VO Module on Virtual KITTI2 Dataset.** Panoptic-Enhanced VO module outperforms DROID-SLAM on most of the highly dynamic VKITTI2 datasets, and the accuracy of the pose estimation is significantly improved after recurrent iterative optimization.

#### A.3.2 Ablation Study of VO-Enhanced VPS Module

As shown in Tab. 7, the online fusion in VO-Enhanced VPS module can help to improve the VPQ results. The recurrent iterative optimization policy can further improve the results. The last two lines of the Tab. 7 indicate that depth can assist in boosting VPQ results.

Methods on VKITT12	Temporal window size				VPQ
	k = 0	k = 5	k = 10	k = 15	
VPS baseline + w/o fusion	58.24 / 60.11 / 57.93	55.50 / 53.78 / 56.28	54.13 / 50.29 / 55.53	53.65 / 48.53 / 55.46	54.90 / 51.95 / 56.05
Ours(VO->VPS + w/o fusion)	58.24 / 60.11 / 57.93	55.67 / 54.44 / 56.28	54.29 / 50.91 / 55.53	53.83 / 49.22 / 55.46	55.04 / 52.48 / 56.05
VPS baseline + w/fusion	59.16 / 67.00 / 56.91	56.27 / 60.98 / 54.96	54.96 / 57.74 / 54.18	54.58 / 55.97 / 54.19	55.81 / 59.23 / 54.85
Ours (VO->VPS + w/fusion + w/o fea loss)	58.51 / 64.07 / 56.97	55.62 / 58.53 / 54.86	54.29 / 55.15 / 54.13	53.94 / 53.40 / 54.19	55.14 / 56.62 / 54.81
Ours (VO->VPS + w/fusion + w/o seg loss)	58.73 / 65.05 / 56.95	55.83 / 59.34 / 54.89	54.51 / 56.01 / 54.15	54.15 / 54.26 / 54.19	55.37 / 57.49 / 54.82
Ours (VO->VPS + w/fusion ) x1	59.18 / 67.00 / 56.94	56.25 / 61.00 / 54.93	54.94 / 57.77 / 54.15	54.57 / 56.01 / 54.17	55.80 / 59.25 / 54.83
Ours (VO->VPS + w/fusion ) x2	<b>59.18</b> / 67.00 / 56.94	<b>56.42</b> / 61.67 / 54.93	<b>55.10</b> / 58.40 / 54.15	<b>54.84</b> / 56.67 / 54.17	<b>55.94</b> / 59.77 / 54.83
Ours (VO->VPS + w/fusion + w/o depth ) x2	59.17 / 66.87 / 56.95	56.39 / 61.45 / 56.25	55.04 / 58.15 / 54.15	54.72 / 56.46 / 54.22	55.89 / 59.57 / 54.83

Table 7: **Ablation Study of our VO-Enhanced VPS module variants on VKITT12 dataset.** Comparison of video panoptic segmentation results. Each cell contains VPQ / VPQ<sup>Th</sup> / VPQ<sup>St</sup> scores. The best results are highlighted in boldface. Our method performs better.

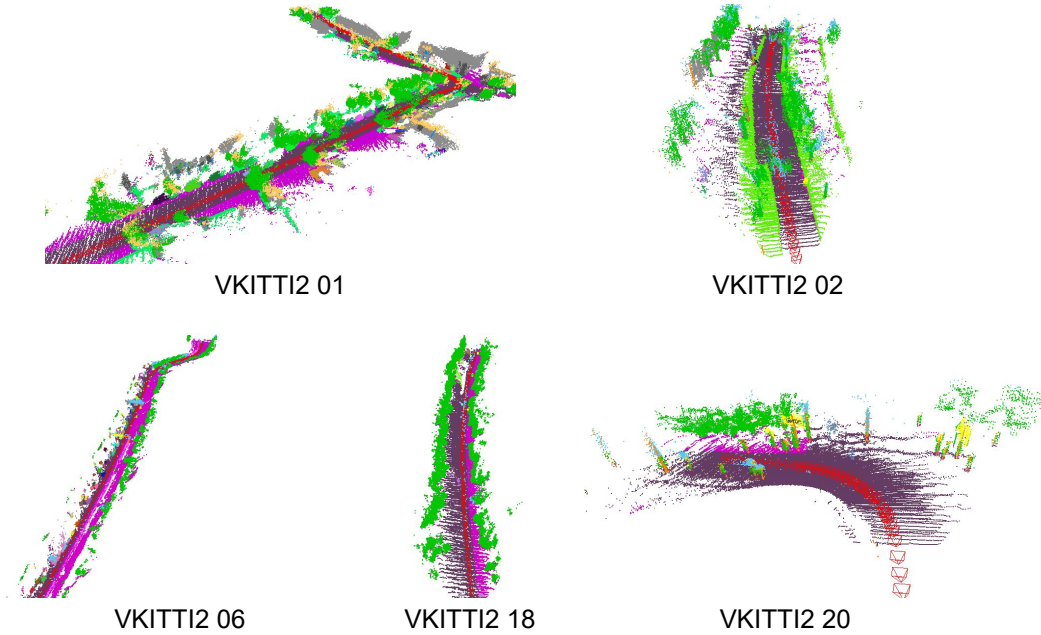
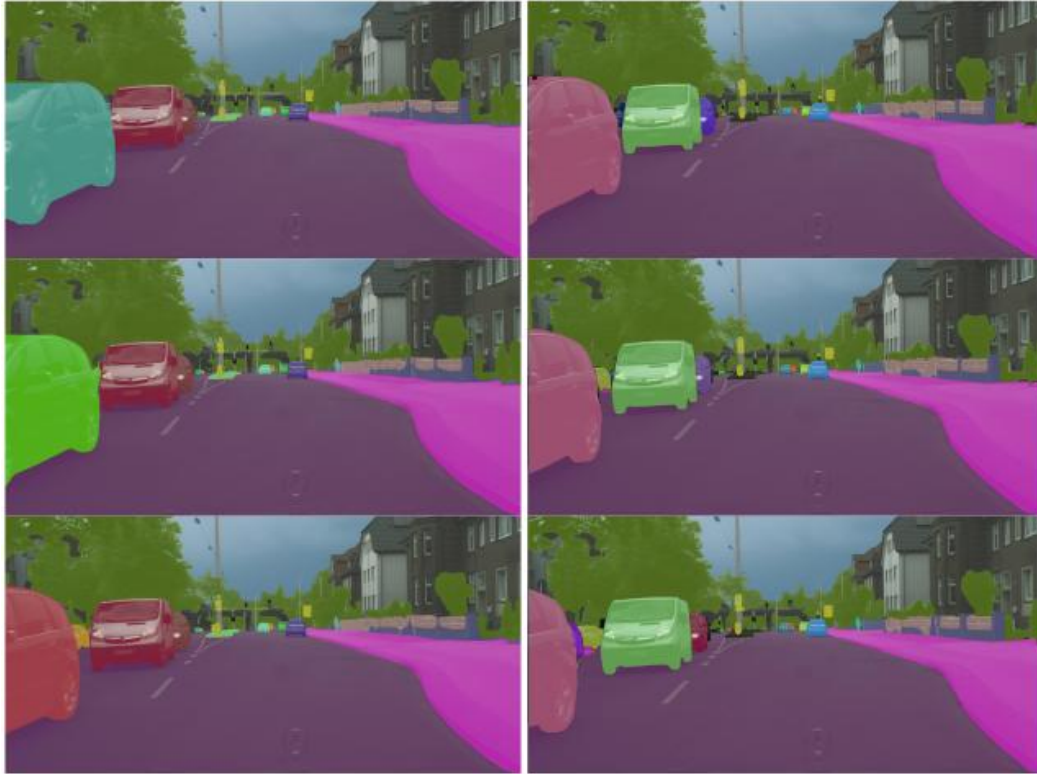


Figure 10: **Qualitative results of panoptic 3D map produced by PVO.** We show the panoptic 3D map produced by our method. The red triangle indicates the camera pose, and different colors indicate different instances.





VPSNet-FuseTrack

Ours

Figure 11: **Comparison results of our methods with VPSNet-FuseTrack [14] on Cityscape-VPS val dataset.** Compared with VPSNet-FuseTrack, our method can keep consistent video segmentation.